

CLS Lattice Performance Analyses

CLS DESIGN NOTE - 8.2.69.1 Rev.0 (formerly 2.1.20B)

Date: 2000-Nov-27

Copyright 2000, Canadian Light Source Inc. This document is the property of Canadian Light Source Inc. (CLS). No exploitation or transfer of any information contained herein is permitted in the absence of an agreement with CLS, and neither the document nor any such information may be released without the written consent of CLS.

Canadian Light Source
107 North Road
University of Saskatchewan
Saskatoon, Saskatchewan Canada

Signature

Date

Original on File – Signed by

Author	_____	_____
	(L.O. Dallin)	
Reviewer #1	_____	_____
	(J.C. Bergstrom)	
Reviewer #2	_____	_____
	(M. de Jong)	
Approver	_____	_____
	(M. de Jong)	

REVISION HISTORY

Revision	Date	Description	Author
A	1999-Jan-06	Original Draft	L.O. Dallin R.M. Silzer D.S. Lowe W.E. Norum
B	1999-Nov-23	Update all changes since January	L.O. Dallin
0	2000-Nov-27	Include Errata in text Correct bunch length Change to 2.9 GeV operation Change file number	L.O. Dallin

Table of Contents

1. Introduction	1
2. Lattice	1
2.1 Tunability.....	5
2.2 The Dynamic Aperture	7
2.3 Orbit Correction Scheme.....	9
2.4 Effects of Insertion Devices.....	11
2.4.1 Analysis of a Superconducting Wiggler	12
2.4.2 Analysis of a Conventional Wiggler	12
2.4.3 Undulators	12
2.4.4 Input Parameters	12
2.4.5 Results	13
2.5 Superconducting Dipoles	15
2.6 The CLS Synchrotron Radiation Characteristics	17
3. References	23

1. Introduction

The Canadian Light Source (CLS) has been designed to operate over an energy range of 1.5 to 2.9 GeV, producing useful synchrotron radiation ranging up to 100 keV. Its lattice parameters define it as one of the new third-generation radiation sources, e.g. the ALS¹ and MAXII²; it has a beam emittance of about 4.8 nm-rad at 1.5 GeV and 18.1 nm-rad at 2.9 GeV.

Our main emphasis was to design a third-generation source, comparable to existing designs, but with a compact lattice. Consequently, the straight sections for insertion devices (IDs) are short, but still have adequate room for the IDs required by the user community.

Lattice independent features such as the vacuum chamber design, bunker temperature, vibration control, feedback systems for orbit control in each beamline, and beam diagnostics are well-documented and easily incorporated in this lattice. Beam lifetimes are studied in a separate report.³

2. Lattice

The compact lattice is composed of twelve identical cells whose structure is a Double Bend Achromat (DBA). Each cell has two dipoles, B, six quadrupoles, Q, and three sextupoles, S, separated by drifts, D. A full cell is shown in Figure 2.1 The dipoles are combined function dipole-quadrupole magnets; the quadrupole component of the dipole magnet supplies vertical focussing in the lattice. The drifts at the ends of each cell, D1, combine to form straight sections (straights) where insertion devices can be located.

The DBA structure was chosen to give the largest number of straights in a compact circumference. The use of combined dipole-quadrupole magnets further reduces the ring size by minimizing the number of separate quadrupole families. Such dipoles are used in the ALS lattice. Separate sextupoles magnets are used. Although such magnets increase the lattice size, they also function as steering coils for orbit control and therefore the space is well utilized.

Lattice design and analyses were done with the code DIMAD⁴. The specifications of the lattice is given in Technical Design Note 2.1.15D.⁵

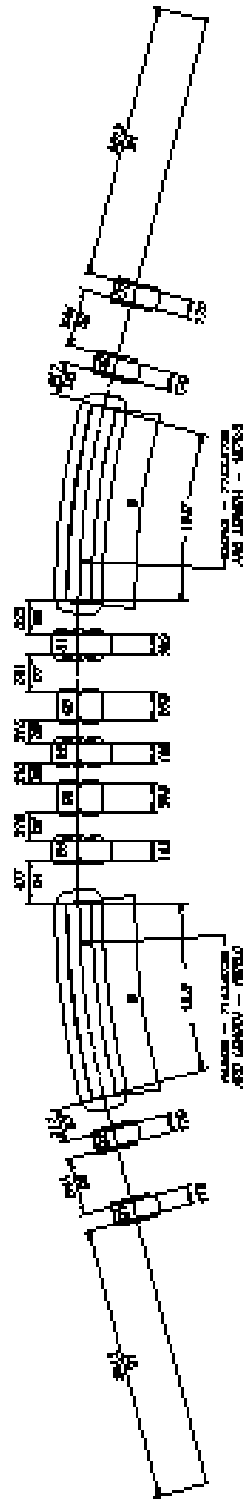


Figure 2.1 Full cell of the CLS (magnet lengths are physical lengths)

The nominal tunes for the lattice are $\nu_x = (10).22$ and $\nu_y = (3).26$. The horizontal emittance (ϵ_x) of the damped beam, when each cell is tuned as an achromat, is 30.6 nm-rad at 2.9 GeV and 8.2 nm-rad at 1.5 GeV. This emittance is reduced (to 18.1 nm-rad at 2.9 GeV) by introducing dispersion ($\eta_x = 0.15$ m) into the straights. The final beam size, σ , is obtained by adding the geometric and chromatic components in quadrature, i.e.,

$$\sigma = \sqrt{\epsilon\beta + \eta^2\delta^2},$$

where $\delta (= \Delta E/E)$ is the damped energy spread of the beam and β the transverse machine function. The machine functions for the lattice with dispersion introduced are shown in Figure 2.2. The corresponding lattice parameters are given in Table 2.1 for three energies: 1.5, 2.5 and 2.9 GeV.

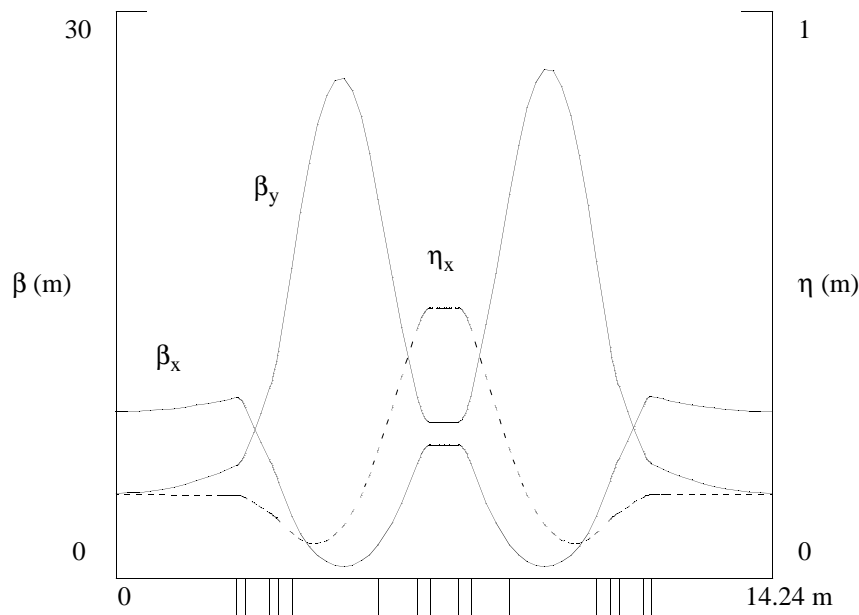


Figure 2.2 Machine functions in one cell for nominal tunes.

Table 2.1 Light Source Parameters for the CLS

Circumference	m	170.88
Periodicity		12
Optics		
v_x (tune)		10.22
v_y		3.26
χ_x (natural chromaticity)		- 13.9
χ_y		- 17.7
momentum compaction		0.0038
Straights		12
length	m	5.2
β_x (betatron amplitude at centre)	m	8.5
β_y	m	4.6
η_x (dispersion)	m	0.15
RF Cavity		
frequency	MHz	500
total voltage	MV	2.4
harmonic number		285
E (energy)	GeV	2.9
B_{dipole}	T	1.354
Damping times		
τ_x	ms	2.4
τ_y	ms	3.8
τ_E	ms	2.7
E-Loss/turn	MeV	0.876
Total Radiated power	kW @500 mA	438
Radiated power/m	kW/m (in dipoles)	9.76
ϵ_x (emittance)	nm-rad	18.1
δ (energy spread)	%	0.111
Energy acceptance	%	1.54
Full bunch length (from tracking)	ps	65

2.1 Tunability

With three families of quadrupoles, the horizontal and vertical tunes and the dispersion in the straight sections can be adjusted. The quadrupole component of the dipole magnets is fixed, but it was initially chosen to optimize the lattice at the nominal tunes. With the dipole gradient fixed, the quadrupoles (Q1, Q2 and Q3) of the optimized lattice were adjusted for a wide range of tunes to check how well the lattice can be tuned. Both the horizontal and vertical tunes were changed over a range of plus or minus one integer, while the dispersion (in the straight sections) was kept fixed at 0.15 m. The results, shown in Table 2.2, indicate a very wide range over which the lattice can be tuned.

The tunability of the lattice in the presence of dipole gradient errors, $\Delta k_{1,\text{dipole}}$, was also investigated. Systematic errors of ± 1 , 2 and 5% were introduced, and the lattice was retuned to the nominal tunes with a dispersion of 0.15 m in the straight sections. The resulting changes in the β -functions (at the centres of the straight sections) and in the emittance are shown in Table 2.3. Random errors up to $\pm 2\%$ in all the dipole gradients were also studied, and the results are also given in Table 2.3. With these errors, the cell-to-cell symmetry in the lattice is broken and β -functions are no longer the same from cell to cell. The random errors result in small changes in β_x but relatively larger changes in β_y from cell to cell. An example is shown in Figure 2.3, where the machine functions for a retuned lattice with $\pm 1\%$ random errors are shown. Such large random errors are not expected but were analyzed to check the tunability of the lattice.

Table 2.2 Large-Scale Tunability

v_x	v_y	Q1 m^{-2}	Q2 m^{-2}	Q3 m^{-2}	β_x m	β_y m	ϵ_x @ 2.9 GeV nm-rad
10.22	3.26	1.688	1.533	1.958	8.5	4.6	18.1
10.22	4.26	1.919	1.147	1.963	9.5	2.7	17.8
10.22	2.26	1.431	1.928	1.953	7.6	7.7	18.6
11.22	3.26	2.028	1.292	2.001	14.8	4.5	13.8
11.22	4.26	2.199	0.962	2.002	16.7	2.6	14.1
11.22	2.26	1.853	1.608	2.000	13.0	7.5	13.5
9.22	3.26	1.153	1.925	1.907	8.1	4.9	29.3
9.22	4.26	1.504	1.422	1.916	9.1	2.8	28.2
9.22	2.26	0.644	2.563	1.893	7.0	8.3	31.1

Table 2.3 Tuning with Dipole Gradient Errors

$\Delta k_{1,dipole}$ %	Q1 m^{-2}	Q2 m^{-2}	Q3 m^{-2}	β_x m	β_y m	ϵ_x nm-rad
0	1.688	1.533	1.958	8.5	4.6	18.1
Systematic						
+1	1.606	1.668	1.958	8.3	4.6	18.2
+2	1.518	1.810	1.958	8.0	4.6	18.2
+5	1.196	2.291	1.955	8.0	4.6	18.6
-1	1.763	1.404	1.958	8.8	4.6	18.1
-2	1.833	1.281	1.958	9.0	4.6	18.1
-5	2.020	0.936	1.958	9.7	4.7	18.1
Random						
± 1 trial a	1.688	1.532	1.959	†	*	18.2
± 1 trial b	1.684	1.538	1.960			18.4
± 2 trial a	1.682	1.539	1.961			18.2
± 2 trial b	1.694	1.520	1.960			18.4

† small variations in β_x * large variations in β_y

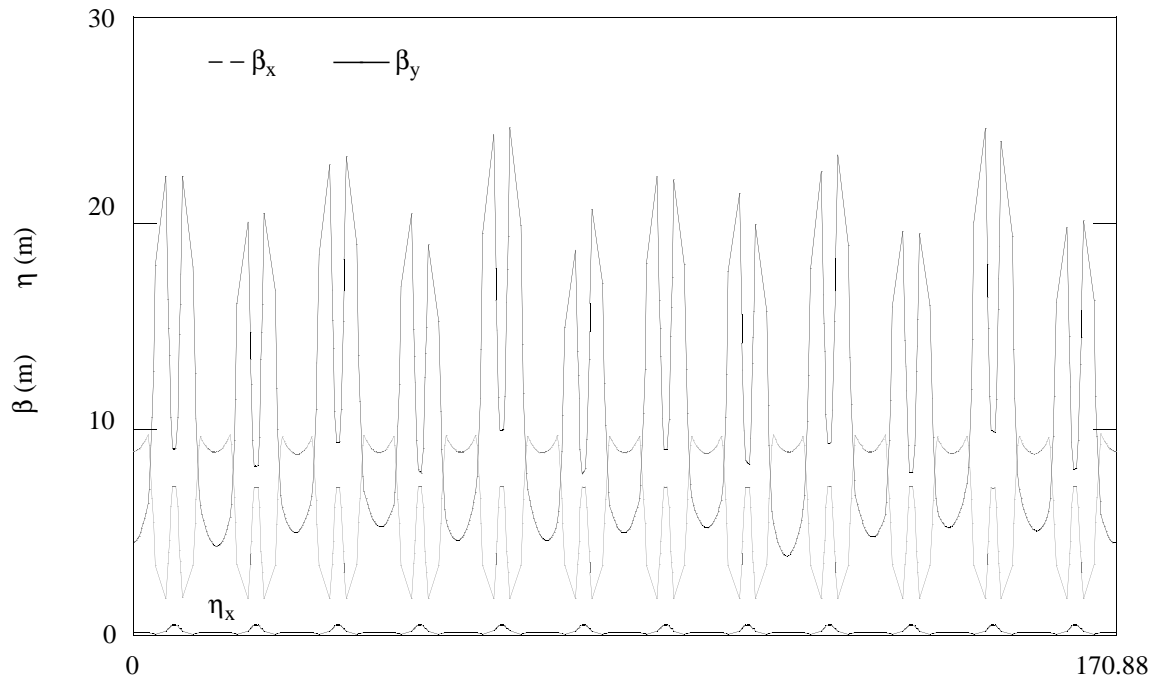


Figure 2.3 Example of machine functions with random dipole gradient errors of 1%.

2.2 The Dynamic Aperture

The dynamic aperture was studied by tracking a single particle for 4000 turns, its initial phase-space coordinates increased until it no longer survived. This number of turns corresponds to about the time for the beam to damp in both transverse directions. The largest “emittance” at which the particle survived was used to define the limit of the dynamic aperture. For calculating beam sizes, the betatron functions at the centres of the straight sections were used.

Several different conditions were studied, and the results are shown in Figure 2.4. First the ideal lattice was studied. Next, multipole fields and misalignments were included in the magnets. A final study was done with misalignments and multipole errors but with the misalignments corrected, as described in the next section. For all the studies, the initial beam “energy,” δ , was taken to be half the damped energy spread, representing an average energy. For a more realistic simulation the full RF voltage was included. Consequently, synchrotron motion caused the energy (δ) to oscillate between positive and negative values. No correction for coupling was included in this study.

Both systematic and random multipole errors were introduced into all the dipole, quadrupole and sextupoles magnets. The errors were the same as estimates made for the SPEAR3 magnets as listed in their conceptual design report.⁶ For the dipole main field, random errors generated from a Gaussian distribution, with an rms value of 0.1% and truncated at 2 sigma, were also introduced.

Transverse misalignments were introduced into the quadrupole and dipole magnets. Random displacements were generated from a Gaussian distribution with an rms value of 200 microns and truncated at 2 sigma. The entrance and the exit of each element was misaligned in both transverse directions. Random longitudinal displacements with an rms value of 500 microns and rotational misalignments (about the beam axis) with an rms value of 500 microradians were also used.

The dynamic aperture of the DBA lattice is shown in Figure 2.4. The effects of all errors we have considered are shown for four random distributions for both the corrected and uncorrected lattice. With misalignments and field errors, the dynamic aperture is reduced, but will still allow the beam orbit to be corrected. The horizontal extent of the dynamic aperture is effectively recovered when the orbit is corrected.

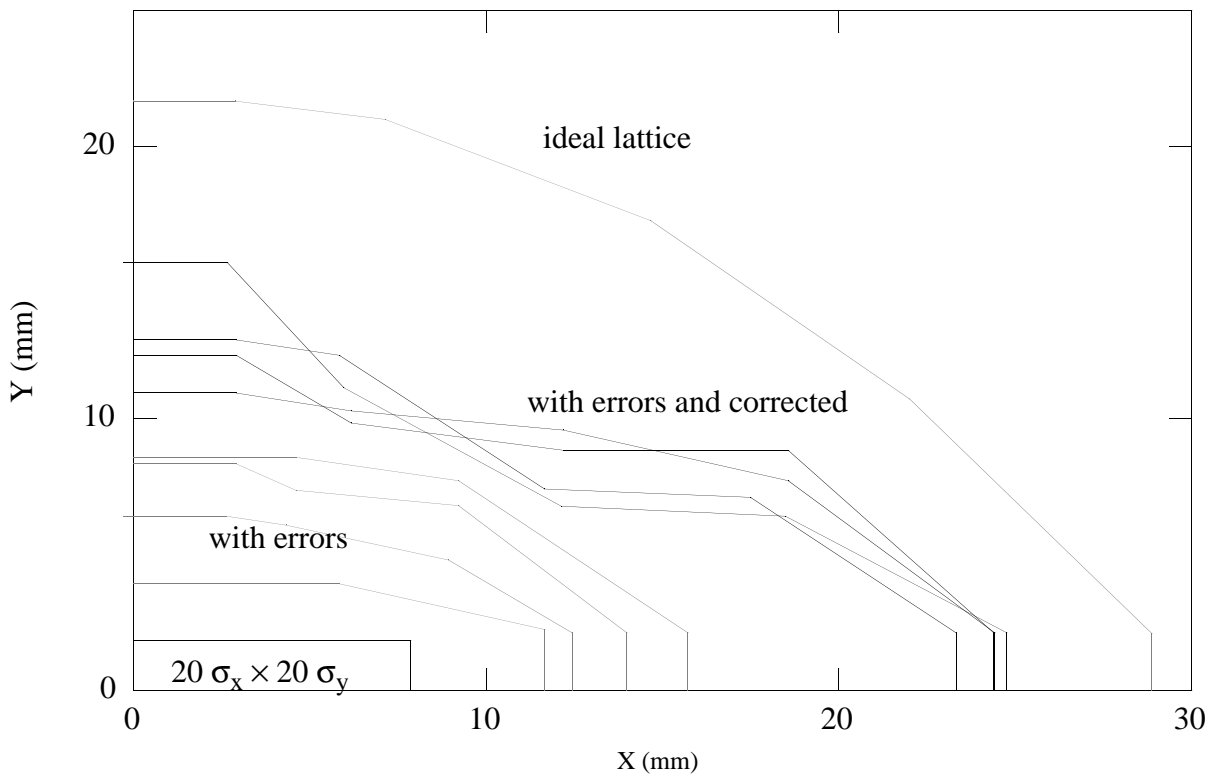


Figure 2.4 Dynamic aperture: results for various lattice conditions.

2.3 Orbit Correction Scheme

Our orbit correction scheme uses dipole windings on the S1 sextupole magnets as well corrector dipoles located between the Q1 and Q2 quadrupoles. The sextupole magnets function as both horizontal correctors (CX) and vertical correctors (CY). The first corrector dipole is a horizontal corrector while the second dipole corrector functions as both a vertical and horizontal corrector. The exact location of the dipole correctors in D2 will be determined by the vacuum chamber design. Each cell has the following configuration of monitors, drift spaces, and correctors (see Figures 2.1 and 2.5):

D1,MHV,Q1,D2(CX4),Q2,D3,B1,MH,D4,S1(CX1,CY1),D5,Q3,D6,S2,
D6,Q3,D7,S1(CX2,CY2),D8,MHV,B2,D3,Q2,D2(CX3,CY3),Q1,MHV,D1

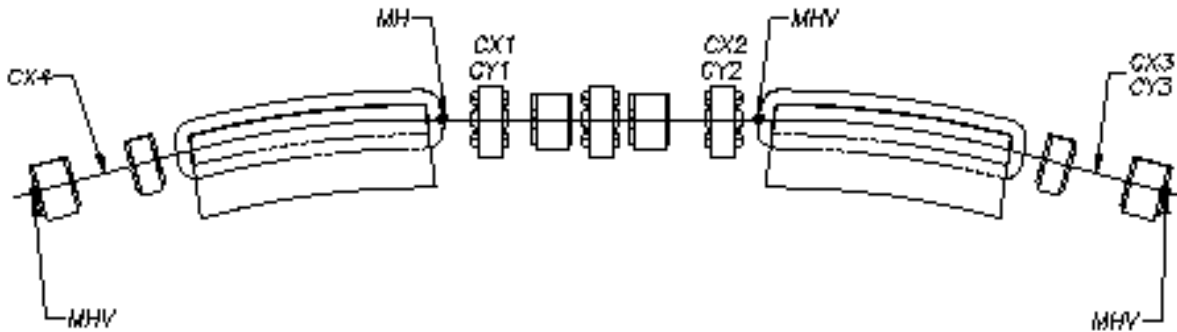


Figure 2.5 Layout of orbit correctors and position monitors.

Four position monitors are employed in each cell. Three of the monitors are both horizontal and vertical sensors (MHV), while the other monitor is a horizontal sensor only (MH). Each cell contains four horizontal monitors and correctors, and three vertical monitors and correctors. This corresponds to over four correctors per 2π phase advance in the horizontal plane and about eleven in the vertical plane.

The orbit correction scheme was studied by introducing the random misalignments described in the previous section. The effects of random monitor misalignments up to 300 microns were also included.

Displacements in the orbit were corrected by using a global orbit correction scheme employing the singular value decomposition algorithm. After correction, the closed orbit of the lattice was

found and used to determine the position of a reference particle at each element in the lattice. From this closed orbit, the RMS beam deviation was determined. Two iterations of the global correction were sufficient to reduce the RMS closed orbits in both planes to values of less than 100 microns in most cases.

The results for ten sets of misalignments are given in Table 2.4, showing the RMS beam deviations and the maximum orbit deviation before and after the orbit correction scheme. The maximum angular “kick” for each correction is also given. The maximum correction never exceeded 0.85 mrad. Typical orbit displacements in the horizontal plane are shown in Figure 2.6.

Table 2.4 Orbit Displacements (Alignment Errors and Monitor Errors)

Trial	Before (mm)				After (μ m)				Kick max (mrad)
	X _{RMS}	Y _{RMS}	X _{max}	Y _{max}	X _{RMS}	Y _{RMS}	X _{max}	Y _{max}	
1	1.89	3.28	3.68	7.60	35.6	46.8	144.5	239.7	0.32
2	2.18	5.66	4.33	17.83	50.2	82.5	141.9	418.1	0.50
3	1.74	4.13	4.11	12.05	34.2	79.1	134.2	435.3	0.53
4	1.38	2.26	3.24	6.77	34.8	78.4	135.6	308.5	0.36
5	1.80	5.84	5.41	12.66	47.6	117.0	249.7	682.4	0.85
6	2.60	2.21	6.01	6.72	43.7	65.0	193.7	270.8	0.40
7	1.59	3.54	4.24	10.35	40.1	80.9	180.0	396.4	0.54
8	3.23	5.91	7.41	18.10	52.2	98.8	195.6	423.2	0.38
9	1.75	5.01	3.52	14.68	36.3	96.5	142.1	448.6	0.41
10	1.24	3.12	3.35	8.47	31.0	69.1	199.8	422.0	0.47
Average	1.94	4.10	4.53	11.52	40.6	81.4	171.7	404.5	0.48

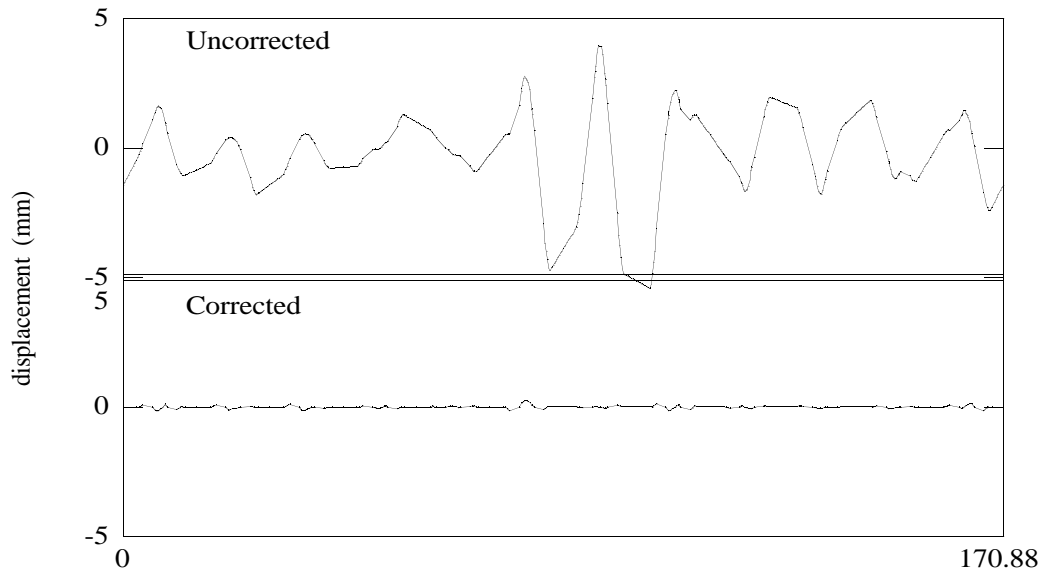


Figure 2.6 Example of uncorrected and corrected horizontal closed orbit displacements.

2.4 Effects of Insertion Devices

The characteristics of the CLS-DBA lattice were evaluated when two wigglers (for hard x-ray production) and four undulators (capable of producing a broad spectrum of synchrotron light) were inserted into six of the lattice straight sections. The optics code DIMAD was used to model each insertion device as a series of full-field poles separated by zero-field drifts. Details of the pole-to-drift ratio, field edge integrals and other optical characteristics are given below. The lattice, including any single insertion device, or all six, proved to be tunable with only a small perturbation to the β -functions around the ring.

The conventional wiggler and undulators are insertion devices (IDs) with many poles. For these IDs, a sinusoidally varying field is assumed. This field is converted to an equivalent hard edge field pattern by using the conditions:

$$W = \frac{4}{\pi^2} \lambda_u \text{ and } B_H = \frac{\pi}{4} B .$$

where W is the width of the hard edge field, B_H is the field strength of hard edge field and B maximum field of the sinusoidal field. λ_u is the ID wavelength.

The distance between poles is given by:

$$D = \frac{\lambda_u}{2} - W.$$

The above definitions for W and B_H satisfy the condition that bend angle and focussing in each pole is the same as a sinusoidal field. The focussing is given by a pole face rotation of half the bend angle at both pole edges.

The various insertion devices and their effect upon the lattice are considered in the following sections.

2.4.1 Analysis of a Superconducting Wiggler

The superconducting wiggler (WS) studied was a three pole device having a central pole field of 5.054 T, with end poles of 2.527 T. At 2.9 GeV the bend angle of the end poles is 0.04 rad while the bend of the centre pole is 0.08 rad. For all poles $W = 0.153$ m.

2.4.2 Analysis of a Conventional Wiggler

For the conventional wiggler (WC), we chose a 17-pole device with a central pole field of 2.112 T and end poles of 1.056 T. The wiggler wavelength, λ_u , is 0.149 m. At 2.9 GeV the bend angle of the end poles is 0.0052 rad and the bend angle of the central poles is 0.0104 rad. For all poles $W = 0.06039$ m.

2.4.3 Undulators

Four undulators (labelled U1, U2, U3 and U4) were also studied. They cover a wide spectrum of possible synchrotron light production. The undulators were modeled with full strength end poles that were one-half the length of the interior poles. The pole lengths and the drift lengths were derived assuming a sinusoidal field.

The undulators, U1, U2 and U4, were assumed to be at low field strength. The remaining insertion device, U3, was taken to be at a high field-strength. The wave lengths and hard edge pole dimensions are given in Table 2.5.

2.4.4 Input Parameters

The parameters for the insertion devices that we examined are summarized in Table 2.5. The “K” value of each undulator is defined as

$$K = 93.4 B \lambda_u,$$

where B is the field in T and λ_u is in m. The K values, gaps and magnetic fields shown in the table are the values used in the simulations. The gaps shown for the undulators are representative of undulators constructed of neodymium-iron permanent magnets. For the wigglers the gaps are arbitrary. The number of poles, N, is shown in two parts, the mid-region and two end poles. The end poles are either half strength or half length. The total length, L, of each ID is also given.

Table 2.5 Light Source ID Parameters

Name	B T	B _H T	λ_u mm	N	gap mm	K	W mm	D mm	L m
WS	5.054	3.969		1	50.8		153.0	35.75	0.534
	2.527	1.985		2					
WC	2.112	1.659	149	15	34.5		60.39	14.11	1.252
	1.056	0.829		2					
U1	0.290	0.228	36	191	21.3	0.98	14.59	3.41	3.456
				2			7.30		
U2	0.218	0.171	48	143	32.9	0.98	19.45	4.55	3.456
				2			9.73		
U3	1.090	0.856	96	71	23.4	9.78	38.91	9.09	3.456
				2			19.45		
U4	0.109	0.086	192	35	184.0	1.95	77.81	18.19	3.456
				2			38.91		

2.4.5 Results

With all six IDs in the CLS lattice, the quadrupoles were adjusted to recover the original transverse tunes of the “bare” lattice. After re-tuning the quadrupoles, the influence of the insertion devices on the β -functions around the ring was examined. The main effect was a distortion of the vertical function (β_y). The dispersions in the straight sections changed slightly. Plots of the β -functions and the dispersion, after the lattice was retuned to accommodate all six insertion devices, are shown in Figure 2.7.

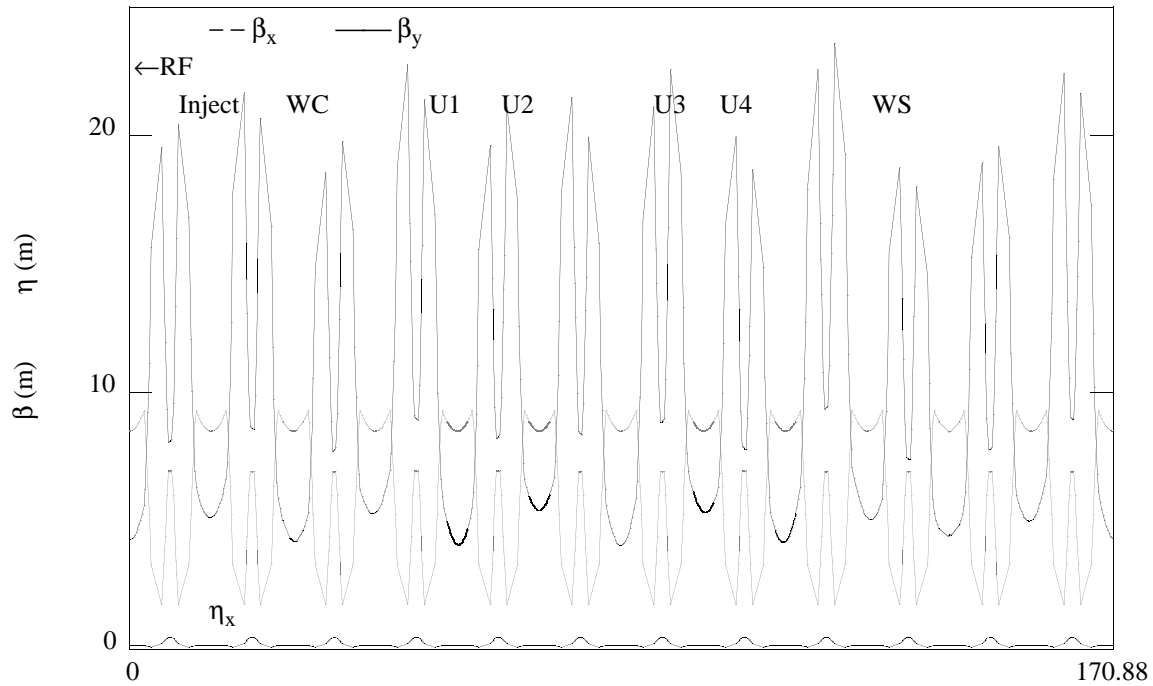


Figure 2.7 Machine functions with insertion devices in the ring.

Details of the source size in each insertion device when all six insertion devices are operating in the lattice are given in Table 2.6. The source size in mm^2 is given by $A = \pi XY$, where $X = (0.001 \epsilon_x \beta_x + 100 \eta_x^2 \delta^2)^{1/2}$ and $Y = (0.0001 \epsilon_x \beta_y)^{1/2}$. The variables, X and Y are in mm, ϵ_x is the damped horizontal emittance in nm-rad, η_x is the horizontal dispersion and δ is the damped relative energy spread in percent. The vertical emittance is assumed to be 10% of the horizontal. The source sizes were calculated in the middle of each straight section where the insertion devices are symmetrically located. Parameters for the straight sections used for injection and for the RF cavity were included in the results. The beam size did not increase by more than 14% from the bare lattice at the position of any of the insertion devices. The bare lattice parameters are also given in Table 2.6.

Table 2.6 Details of Source Size with Six IDs in Lattice (@ 2.9 GeV).

Position	ϵ_x nm-rad	β_x m	β_y m	η_x m	δ %	X mm	Y mm	A mm ²
RF	18.8	8.5	4.3	0.150	0.116	0.44	0.090	0.123
Inject	18.8	8.5	5.1	0.150	0.116	0.44	0.098	0.134
WC	18.8	8.5	4.2	0.150	0.116	0.44	0.089	0.122
U1	18.8	8.5	4.1	0.150	0.116	0.44	0.088	0.120
U2	18.8	8.5	5.4	0.150	0.116	0.44	0.101	0.138
U3	18.8	8.5	5.3	0.150	0.116	0.44	0.100	0.137
U4	18.8	8.5	4.2	0.150	0.116	0.44	0.089	0.122
WS	18.8	8.5	4.5	0.156	0.116	0.44	0.092	0.127
Bare	18.1	8.5	4.6	0.150	0.111	0.43	0.091	0.122

Note: The configuration of insertion devices shown here is not the final configuration planned for the CLS. The analyses here merely serves to indicate the sort of optics distortions that a large number of devices would generate. It is interesting to note that most of the perturbation to the lattice comes from WS. Excluding this ID from the analysis results in variations in β_y ranging from 4.4 to 4.9. As well, with no SC wiggler, the emittance decreases to 17.9 nm-rad.

2.5 Superconducting Dipoles

We have also investigated the possibility of obtaining additional hard x-ray ports by replacing some of the ring dipole magnets with superconducting (SC) dipoles. SC dipoles of 4.06 T are considered. To preserve the symmetry of a given cell both dipoles in a cell are replaced. The SC dipole gradients are set to zero and the vertical focussing normally supplied by the dipole is supplied by two quadrupoles (Q4) surrounding the SC dipole. The four quadrupole families in the cell are used to adjust the new SC cell. Both horizontal and vertical tunes, the horizontal β -function and horizontal dispersion are matched to a normal cell. A small vertical β -function mismatch causes some perturbation to the machine functions around the ring.

The effects of adding two or four SC dipoles to the lattice are shown in Table 2.7. In the case of four SC additions, the SC dipoles are located diametrically opposite to each other in the ring. The effect of the vertical mismatch is shown in Figure 2.8 for the case of two SC dipoles.

Table 2.7 Effects of Substituting SC Dipoles in the Ring

Number of SC dipoles	0	2	4
Field strength (T)	-	4.06	4.06
Gradient, k (m ⁻²)	-	0.0	0.0
Q1 k (m ⁻²)	1.688	1.911	1.911
Q2 k (m ⁻²)	1.534	1.154	1.154
Q3 k (m ⁻²)	1.958	1.972	1.972
Q4 k (m ⁻²)	-	- 1.805	- 1.805
v _x	10.22	10.22	10.22
v _y	3.26	3.26	3.26
ε _x (nm-rad)	18.1	23.9	28.9
δ _x (%)	0.111	0.127	0.136

In contrast to insertion devices, SC dipoles allow the entrance of an x-ray beamline to be located nearly at the source where the beamline acceptance is maximum. The energy spectrum from the SC dipoles will be similar to that of the SC wiggler described earlier. The drawback to adding SC dipoles to the lattice is that the brightness of the ring is reduced by about 25% (if two are added) and by about 40% (if four are added) because of the increase in beam emittance and energy spread.

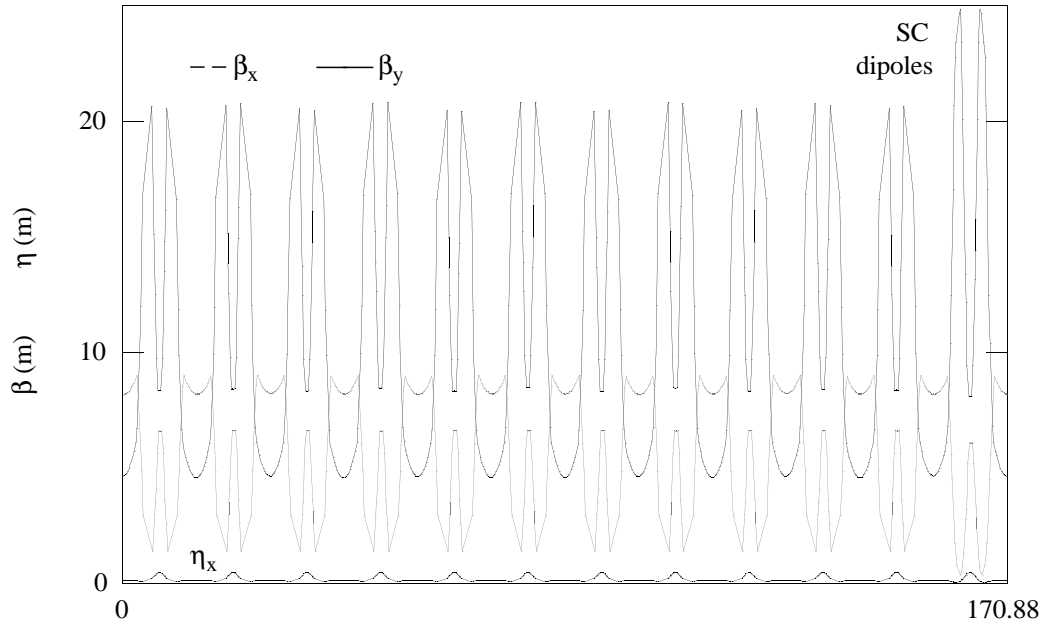


Figure 2.8 Effect of two SC dipoles on the machine functions

2.6 The CLS Synchrotron Radiation Characteristics

The brightness associated with the dipoles and insertion devices described in Table 2.5 are plotted in Figure 2.9. (10% vertical coupling is assumed.) The elements are:

- Dipole magnet radiation, which is shown for two operating energies. Note that the maximum brightness is nearly independent of beam energy since, except for small differences in energy spread, it is proportional to E^2/ϵ_x . The critical energy, ϵ_c , of the radiation is 1.05 and 7.57 keV for operating energies of 1.5 and 2.9 GeV respectively.
- The undulators listed in Table 2.5. The curves are the loci of the possible light output over a range of undulator K values ranging from a K of one to K about $0.1\lambda_u$ (λ_u in mm) and using the first three odd harmonics.
- Two wigglers, the lower field one slightly reduced in strength from that listed in Table 2.5. The fields are 1.4 and 5.1 T with critical energies (at 2.9 GeV) of 7.8 and 28.5 keV respectively. The SC wiggler can be used to generate very hard x-rays. Since the spectrum is useful up to four times the critical energy, 100 keV x-rays will be available at the maximum design energy of 2.9 GeV.

- A short period (20 mm) undulator for high brightness, hard x-rays, using odd harmonics up to $n=15$. A ID length of 3.5 m was used.

The characteristics of the CLS at 1.5 GeV compare favourably with the new third-generation light sources at Berkeley (ALS) and Lund (MAX II) which are described in Table 2.8. At this operating energy our lattice has comparable emittance and consequently equivalent brightness at the same operating current. Our additional capability to operate up to 2.9 GeV enables us to produce hard x-rays, *making our design a unique facility for Canadian researchers and industrial users.*

The brightness curves for the CLS, ALS and MAX II machines are shown in Figure 2.10 for an operating energy of 1.5 GeV. The output from the same insertion device (the conventional wiggler) and the radiation from a dipole magnet, are compared. The CLS lattice, with its 12 straight sections, is an extremely cost effective, competitive design.

For the dipole calculations, the β functions in the dipoles were used to calculate the beam size. In the MAX II and CLS lattices, the beam size is the same in all dipoles. For the ALS lattice, the beam size is smaller in the center dipole in each triple bend achromat (TBA), and these dipoles were used for the plots in Figure 2.10.

Finally, the photon flux from the dipoles and wigglers of an operating energy of 2.9 GeV is shown in Figure 2.11. In terms of flux, the superconducting wiggler is an excellent source of x-rays up to 100 keV.

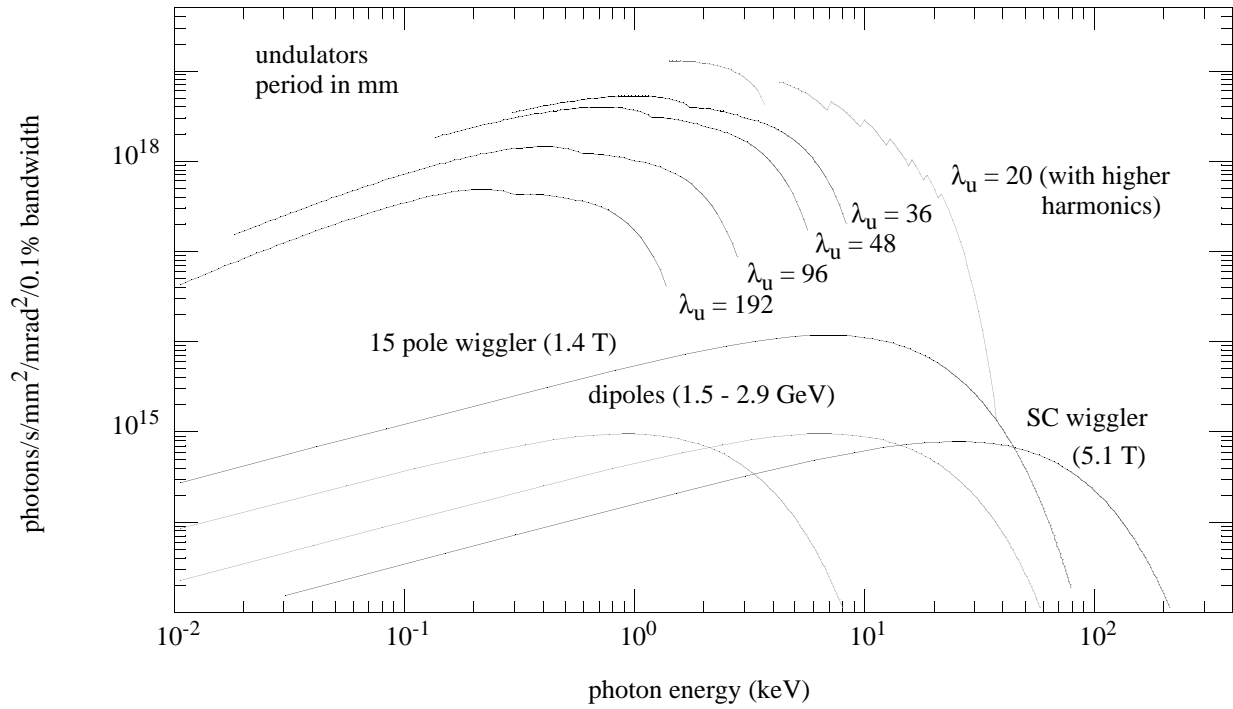


Figure 2.9 Brightness vs. photon energy from the light source dipoles for two operating energies and for IDs at 2.9 GeV.

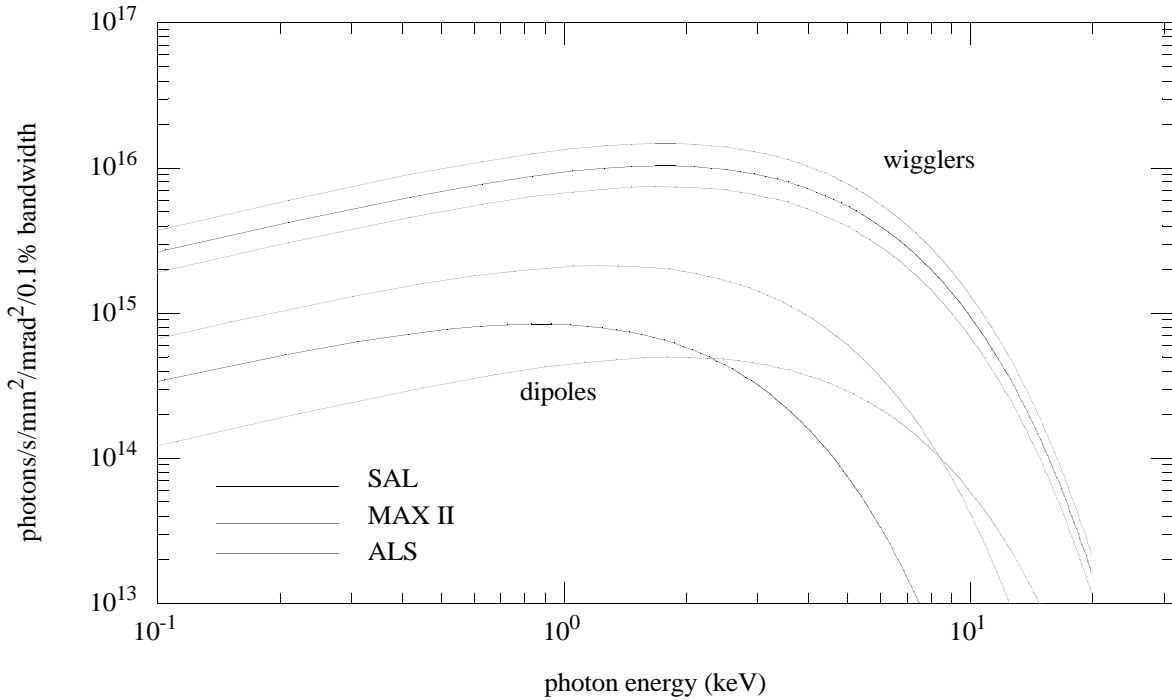


Figure 2.10 Comparison of brightness for the CLS, ALS and MAX II machines at 1.5 GeV. The 15-pole wiggler from Figure 2.9 is used for these comparisons.

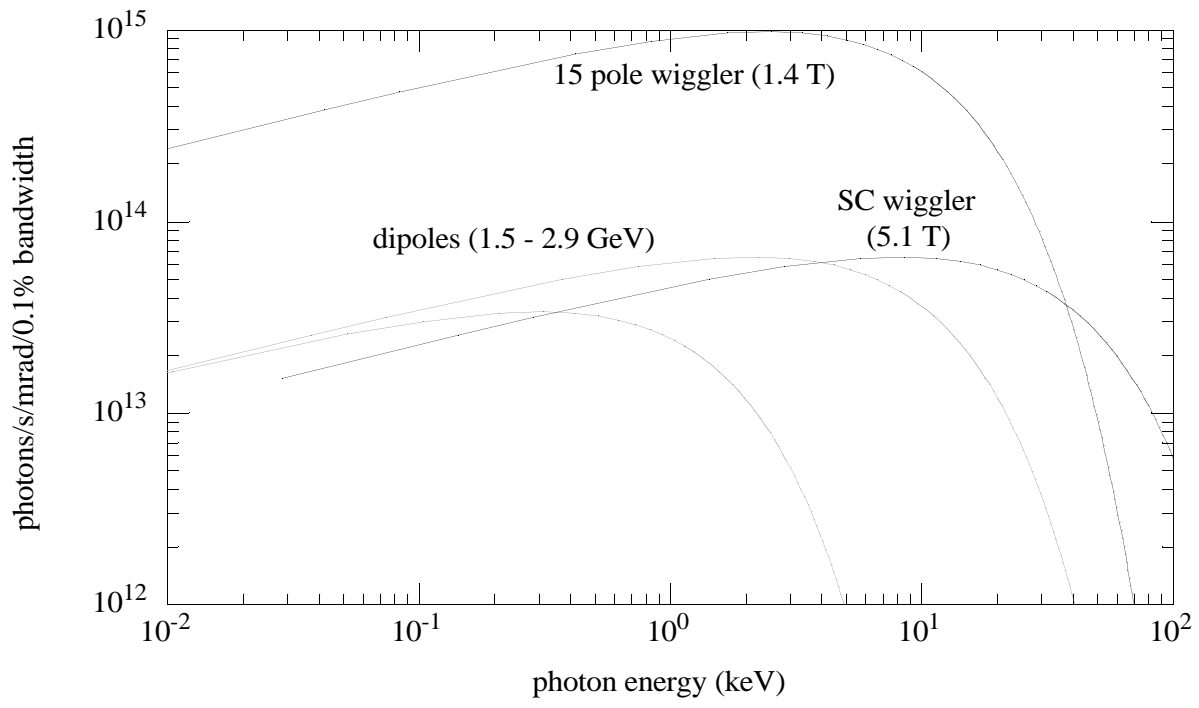


Figure 2.11 Spectral flux vs. photon energy from the light source dipoles for two operating energies and for two wigglers at 2.9 GeV.

Table 2.8 Comparison of the CLS, ALS and MAX II lattices at 1.5 GeV

	CLS	ALS	MAX II
Dipoles	24 x 1.87 m 0.700 T k = -0.400	36 x 0.854 m 1.022 T k = -0.819	20 x 1.047 m 1.501 T k = 0
Quadrupoles	48 x 0.194 m 24 x 0.277 m	48 x 0.2 m 24 x 0.35m 24 x 0.5 m	20 x 0.25 m 20 x 0.2 m 20 x 0.18 m 10 x 0.5 m
Sextupoles	36 x 0.21 m	48 x 0.2 m	included in quads
Total magnetic length (m)	68.40	70.344	38.54
Total length (m)	170.9	196.8	90.0
Tunes ν_x ν_y	10.22 3.26	14.281 8.199	9.221 3.262
Emittance ϵ_x (nm-rad)	4.8	3.4	8.3
$\delta = \Delta E/E$ (%)	0.057	0.065	0.071
Drift space parameters Length (m) (values at centre) β_x (m) β_y (m) η_x (m)	12 x 5.2 8.5 4.6 0.15	12 x 6.75 12.2 4.1 0.0	10 x 3.14 11.5 2.2 0.16
Horizontal beam size (mm) $\sqrt{0.001 \epsilon_x \beta_x + 100 \eta_x^2 \delta^2}$	0.22	0.20	0.42
Vertical beam size (mm) (10% coupling) $\sqrt{0.0001 \epsilon_x \beta_y}$	0.047	0.037	0.043

3. References

1. 1-2 GeV Synchrotron Radiation Source. Conceptual Design Report, LBL PUB-5172 Rev. (1986).
2. A. Andersson, O. Cederholm, M. Eriksson, L.G. Johansson, L.J. Lindgren, M. Nilsson, P. Rojsel, W. Stiefeler, T. Svensson, J. Tagger, L. Thanell and S. Werin. Design Report for the MAX II Ring, MAX-lab, University of Lund, ISSN 0284-1258 (1992).
3. R. M. Silzer, "CLS Beam Lifetime Studies", CLS Technical Design Note 2.1.19C (in progress)
4. R. V. Servranckx, "USERS' GUIDE TO THE PROGRAM DIMAD", TRIUMF-DN -93-K233
5. L. O. Dallin, "Canadian Light Source Main Ring Lattice", CLS Technical Design Note 2.1.15D
6. SPEAR3 Conceptual Design Report, last revised: 7/14/98.